INTERACTION OF A FLEXIBLY SUPPORTED AIRFOIL AND A CHANNEL FLOW

Miloslav Feistauer*, Jaromír Horáček**, Martin Růžička*, Petr Sváček***

The subject of the paper is the numerical simulation of the interaction of two-dimensional incompressible viscous flow and a vibrating airfoil inserted in a channel (e.g. wind tunnel). A solid airfoil with two degrees of freedom can rotate around the elastic axis and oscillate in the vertical direction. The numerical simulation consists of the finite element solution of the Navier-Stokes equations coupled with the system of ordinary differential equations describing the airfoil motion. The time dependent computational domain and a moving grid are taken into account with the aid of the Arbitrary Lagrangian-Eulerian (ALE) formulation of the Navier-Stokes equations. High Reynolds numbers up to 10^6 *require the application of a suitable stabilization of the finite element discretization. Numerical results are compared with an experiment.*

Key words: *aeroelasticity, finite element metod, Arbitrary Lagrangian-Eulerian formulation, stabilization for high Reynolds numbers*

1. Introduction

The interaction of fluids and structures plays an important role in many fields of science and technology. The research in aeroelasticity or hydroelasticity focuses on the interaction between flowing fluids and vibrating structures (see, e.g. [4] and [15]). The aeroelastic stability of aerospace vehicles and the aeroelastic responses represented by dynamic load prediction and vibration levels in wings, tails and other aerodynamic surfaces have a great impact on the design as well as in the cost and operational safety.

In [19] we analyzed numerically the interaction of a moving fluid with an isolated airfoil. In many cases it is necessary to compare computational results with wind tunnel experiments. It appears that the bounded height of the wind tunnel measurement section influences the flow field past the airfoil as well as the structural behaviour of the airfoil. Therefore, we are concerned here with the numerical analysis of flow induced vibrations of the airfoil inserted into a channel representing the measurement section of a wind tunnel. We consider a two-dimensional viscous incompressible channel flow past a moving airfoil, which is considered as a solid body with two degrees of freedom, allowing its vertical and torsional oscillations taking into account the changes of the flow region around the airfoil during the vibration.

* M. Feistauer, M. Růžička, Faculty of Mathematics and Physics, Charles University Prague, Sokolovská 83, 186 75 Praha 8, Czech Republic

** J. Horáček, Institute of Thermomechanics, Academy of Sciences of the Czech Republic, Dolejškova 5, 182 00 Praha 8, Czech Republic

*** P. Sváček, Department of Technical Mathematics, Faculty of Mechanical Engineering, Czech Technical University Prague, Karlovo n. 13, 121 35 Praha 2, Czech Republic

The numerical simulation consists of the finite element solution of the Navier-Stokes equations coupled with the system of ordinary differential equations describing the airfoil motion. The time dependent computational domain and a moving grid are taken into account with the aid of the Arbitrary Lagrangian-Eulerian (ALE) formulation of the Navier-Stokes equations.

By $Re = UL/\nu$ we denote the Reynolds number, where U is a reference velocity (in our case the inlet velocity), L is the length of the airfoil and ν is the kinematic viscosity. The Reynolds numbers in relevant applications are quite large, namely between 10^5 and 10^6. (For such regimes the flow is usually turbulent, but here we simulate the flow with the aid of the classical Navier-Stokes equations without any turbulence model.) For the solution of such flows it is necessary to use very accurate and robust finite element schemes. In oder to avoid spurious oscillations, the SUPG (streamline upwind Petrov-Galerkin) and div-div stabilization methods are applied. The solution of the ordinary differential equations is carried out by the Runge-Kutta method. Special attention is paid to the construction of the ALE mapping of a reference domain on the computational domain at individual time instants. The resulting nonlinear discrete algebraic system is solved by the Oseen iterative process. As a result we obtained a sufficiently accurate and robust method for the numerical simulation of flow induced vibrations of an airfoil inserted in a wind tunnel. The method was tested on a problem for which experimental results are available. The comparison of computational and experimental results shows a good agreement.

2. Formulation of a flow problem in a moving domain

We assume that $(0,T)$ with $T > 0$ is a time interval and by Ω_t we denote a computational domain occupied by the fluid at time t. It represents a channel (e.g. wind tunnel) with an inserted vibrating airfoil. By $\mathbf{u} = \mathbf{u}(x,t)$ and $p = p(x,t)$, $x \in \Omega_t$, $t \in (0,T)$, we denote the velocity and the kinematic pressure (i.e., the dynamic pressure divided by the density of the fluid), respectively, and ν will denote the kinematic viscosity.

In order to simulate flow in a moving domain, we employ Arbitrary Eulerian-Lagrangian (ALE) method ([16]). This technique is based on a one-to-one smooth mapping $\mathcal{A}_t$ of a reference domain Ω_{ref} onto the computational domain Ω_t at time t. (Usually we set $\Omega_{\mathrm{ref}} = \Omega_0$.) Thus, each $X \in \Omega_{\mathrm{ref}}$ is associated with $x = x(X,t) = \mathcal{A}_t(X) \in \Omega_t$.

Based on this mapping we can compute the *domain velocity* $\tilde{\mathbf{w}}$ at all points X of the reference configuration Ω_{ref} for each time level:

$$\tilde{\mathbf{w}}(X,t) = \frac{\partial}{\partial t}\, x(X,t)\ , \tag{1}$$

which can be transformed to the space coordinates x by the relation

$$\mathbf{w}(x,t) = \tilde{\mathbf{w}}(\mathcal{A}_t^{-1}(x),t)\ . \tag{2}$$

With the aid of the ALE mapping we compute the so-called *ALE derivative* $D^{\mathcal{A}}/Dt$, which is anologous to the *material derivative* in the Lagrangian approach. For a function $f = f(x,t)$, $x \in \Omega_t$, $t \in (0,T)$, we define the function $\tilde{f}(X,t) = f(\mathcal{A}_t(X),t)$, $X \in \Omega_{\mathrm{ref}}$, $t \in (0,T)$, and set

$$\frac{D^{\mathcal{A}}}{Dt}\, f(x,t) = \frac{\partial \tilde{f}}{\partial t}(X,t)\ , \qquad X = \mathcal{A}_t^{-1}(x)\ . \tag{3}$$

We find that

$$\frac{D^{\mathcal{A}}}{Dt} f = \frac{\partial f}{\partial t} + (\mathbf{w} \cdot \nabla) f \ . \tag{4}$$

Now we reformulate the Navier-Stokes equations in the ALE form

$$\frac{D^{\mathcal{A}}}{Dt} \mathbf{u} + [(\mathbf{u} - \mathbf{w}) \cdot \nabla] \mathbf{u} + \nabla p - \nu \triangle \mathbf{u} = 0 \quad \text{in} \quad \Omega_t \ , \tag{5}$$

$$\nabla \cdot \mathbf{u} = 0 \quad \text{in} \quad \Omega_t \ . \tag{6}$$

This system is equipped with the initial condition

$$\mathbf{u}(x, 0) = \mathbf{u}_0 \ , \quad x \in \Omega_0 \ , \tag{7}$$

and boundary conditions. We assume that $\partial\Omega_t = \Gamma_{\mathrm{D}} \cup \Gamma_{\mathrm{O}} \cup \Gamma_{\mathrm{W}t}$, where Γ_{D},Γ_{O} and $\Gamma_{\mathrm{W}t}$ are mutually disjoint. On Γ_{D}, representing the inlet and impermeable fixed walls of the channel, we prescribe the Dirichlet boundary condition

$$\mathbf{u}|_{\Gamma_{\mathrm{D}}} = \mathbf{u}_{\mathrm{D}} \ . \tag{8}$$

On the walls, $\mathbf{u}_{\mathrm{D}} = 0$. We denote by $\Gamma_{\mathrm{W}t}$ the boundary of the airfoil at time t. On $\Gamma_{\mathrm{W}t}$ we assume that the fluid velocity $\mathbf{u}$ equals the velocity $\tilde{\mathbf{u}}_\Gamma$ of the profile:

$$\mathbf{u}|_{\Gamma_{\mathrm{W}t}} = \tilde{\mathbf{u}}_\Gamma = \mathbf{w}|_{\Gamma_{\mathrm{W}t}} \ . \tag{9}$$

The part Γ_{O} of the boundary represents the outlet, where we prescribe the 'do-nothing' boundary condition

$$-(p - p_{\mathrm{ref}})\, \mathbf{n} + \nu \frac{\partial \mathbf{u}}{\partial \mathbf{n}} = 0 \quad \text{on} \quad \Gamma_{\mathrm{O}} \ . \tag{10}$$

Here $\mathbf{n}$ is the unit outer normal to $\partial\Omega_t$ and p_{ref} is a prescribed reference outlet pressure.

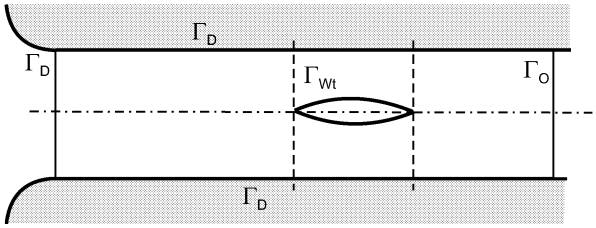

Fig.1: Airfoil in a channel

3. Description of the airfoil motion

We assume that the airfoil is a dynamic system with two degrees of freedom. This means that we consider the airfoil as a solid body, which can oscillate in the vertical direction and in the angular direction around the so-called elastic axis denoted by EO, see Figure 2. The displacement h is oriented positively with the coordinate x_2. The rotation angle α is oriented positively in the clockwise direction.

The linearized equations describing the motion of the airfoil were derived, e.g. in [4] from the Lagrange equations and can be written in the matrix form

$$\widehat{\mathbf{K}}\,\mathbf{d}(t) + \widehat{\mathbf{B}}\,\dot{\mathbf{d}}(t) + \widehat{\mathbf{M}}\,\ddot{\mathbf{d}}(t) = \widehat{\mathbf{f}}(t)\ , \tag{11}$$

where the stiffness matrix $\widehat{\mathbf{K}}$, the viscous structural damping $\widehat{\mathbf{B}}$ and the mass matrix $\widehat{\mathbf{M}}$ have the form

$$\widehat{\mathbf{K}} = \begin{pmatrix} k_{hh} & k_{h\alpha} \\ k_{\alpha h} & k_{\alpha\alpha} \end{pmatrix}\ , \qquad \widehat{\mathbf{B}} = \begin{pmatrix} D_{hh} & D_{h\alpha} \\ D_{\alpha h} & D_{\alpha\alpha} \end{pmatrix}\ , \qquad \widehat{\mathbf{M}} = \begin{pmatrix} m & S_\alpha \\ S_\alpha & I_\alpha \end{pmatrix}\ .$$

The vector of the force $\widehat{\mathbf{f}}$ and the vector $\mathbf{d}$ of generalized coordinates are given by

$$\widehat{\mathbf{f}}(t) = \begin{pmatrix} -\mathcal{L}(t) \\ \mathcal{M}(t) \end{pmatrix}\ , \qquad \mathbf{d}(t) = \begin{pmatrix} h(t) \\ \alpha(t) \end{pmatrix}\ .$$

The symbol $\mathcal{L}$ denotes the component of the force acting on the airfoil in the vertical direction x_2, $\mathcal{M}$ is the torsional moment of the force with respect to the elastic axis, D_{hh}, $D_{h\alpha}$, $D_{\alpha h}$, $D_{\alpha\alpha}$ are the coefficients of the viscous structural damping. Further, S_α, I_α, m and k_{hh}, $k_{\alpha\alpha}$, $k_{h\alpha}$, $k_{\alpha h}$ denote the static moment around the elastic axis EO, the moment of inertia around EO, the mass of the profile and the stiffness coefficients of the profile, respectively.

The functions $\mathcal{L}$ and $\mathcal{M}$ acting on the profile with a depth ℓ are given by the relations

$$\mathcal{L} = -\ell \int\limits_{\Gamma_{\mathrm{W}_t}} \sum_{j=1}^{2} T_{2j}\, n_j \,\mathrm{d}s\ , \tag{12}$$

$$\mathcal{M} = \ell \int\limits_{\Gamma_{\mathrm{W}_t}} \sum_{i,j=1}^{2} T_{ij}\, n_j (-1)^i \left(x_{1+\delta_{1i}} - x^{\mathrm{EO}}_{1+\delta_{1i}}\right) \mathrm{d}s\ , \tag{13}$$

where $\mathbf{n} = (n_1, n_2)$ is the unit outer normal to $\partial\Omega_t$ on Γ_{W_t} and δ_{ij} is the Kronecker symbol, i.e. $\delta_{ij} = 1$ for $i = j$ and $\delta_{ij} = 0$ for $i \neq j$, x_1, x_2 are the coordinates of points on Γ_{W_t} and x_i^{EO}, $i = 1{,}2$, are the coordinates of the elastic axis EO. Further,

$$T_{ij} = \rho \left[-p\,\delta_{ij} + \nu \left(\frac{\partial u_i}{\partial x_j} + \frac{\partial u_j}{\partial x_i} \right) \right]\ . \tag{14}$$

Relations (12)–(14) represent the coupling of the flow problem and structural problem.

System (11) is equipped with the initial conditions

$$\begin{aligned} \alpha(0) &= \alpha_0\ , \qquad & \dot{\alpha}(0) &= \alpha_1\ , \\ h(0) &= h_0\ , \qquad & \dot{h}(0) &= h_1\ , \end{aligned} \tag{15}$$

where α_0, α_1, h_0, h_1 are input data of the problem.

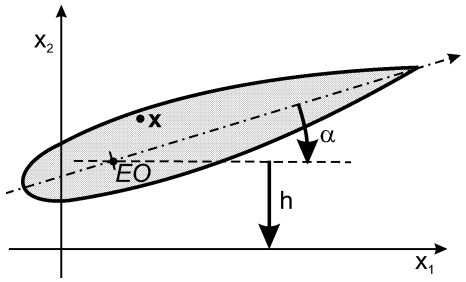

Fig.2: Airfoil with two degrees of freedom

4. Discretization of the flow problem

There is a number of possibilities how to carry out the space-time discretization ([8], [20]). In order to develop a stable, accurate scheme, which can easily treat complicated boundaries, we apply the finite element method (FEM). For obtaining a physically acceptable numerical solution, it is not possible to use a standard Galerkin FEM, but we have to introduce a suitable stabilization. Here we apply the *streamline diffusion method* (also called SUPG method) together with *div-div* stabilization of the pressure, following [9], [14].

4.1. Time discretization

First let us describe the time discretization of the flow problem. We consider a partition $0 = t_0 < t_1 < \cdots < T$, $t_k = k\,\Delta t$, with a time step $\Delta t > 0$, of the time interval $[0, T]$ and approximate the solution $\mathbf{u}(t_n)$ (defined in Ω_{t_n}) at the time instant t_n by $\mathbf{u}^n$. For the time discretization we use the second-order two-step backward difference formula using the computed approximate solution $\mathbf{u}^{n-1}$ in $\Omega_{t_{n-1}}$ and $\mathbf{u}^n$ in Ω_{t_n} for the calculation of $\mathbf{u}^{n+1}$ defined in the domain $\Omega_{t_{n+1}}$. With the given ALE mapping $\mathcal{A}_t$ we have

$$\mathcal{A}_{t_{n-1}}(X) = x^{n-1} \in \Omega_{t_{n-1}}\ , \quad \mathcal{A}_{t_n}(X) = x^n \in \Omega_{t_n}\ , \quad \mathcal{A}_{t_{n+1}}(X) = x^{n+1} \in \Omega_{t_{n+1}}\ , \tag{16}$$

where $X \in \Omega_{\mathrm{ref}}$ is a given point from the reference configuration, e.g. a node of the triangulation.

Now we define the approximation of the ALE derivative at time t_{n+1} and point x^{n+1} by

$$\begin{aligned}\frac{D^{\mathcal{A}}\mathbf{u}}{Dt}(x^{n+1}, t_{n+1}) &\approx \frac{3\,\tilde{\mathbf{u}}^{n+1}(X) - 4\,\tilde{\mathbf{u}}^{n}(X) + \tilde{\mathbf{u}}^{n-1}(X)}{2\,\Delta t} = \\ &= \frac{3\,\mathbf{u}^{n+1}(x^{n+1}) - 4\,\mathbf{u}^{n}(x^{n}) + \mathbf{u}^{n-1}(x^{n-1})}{2\,\Delta t}\ .\end{aligned} \tag{17}$$

and obtain the problem for the unknown functions $\mathbf{u}^{n+1} \colon \Omega_{t_{n+1}} \to R^2$ and $p^{n+1} \colon \Omega_{t_{n+1}} \to R$:

$$\begin{aligned}&\frac{3\,\mathbf{u}^{n+1}(x^{n+1}) - 4\,\mathbf{u}^{n}(x^{n}) + \mathbf{u}^{n-1}(x^{n-1})}{2\,\Delta t} + \\ &\quad + \Big(\big(\mathbf{u}^{n+1}(x^{n+1}) - \mathbf{w}^{n+1}(x^{n+1})\big)\cdot\nabla\Big)\,\mathbf{u}^{n+1}(x^{n+1}) - \\ &\qquad - \nu\,\Delta\mathbf{u}^{n+1}(x^{n+1}) + \nabla p^{n+1}(x^{n+1}) = 0\ , \\ &\qquad \operatorname{div}\mathbf{u}^{n+1}(x^{n+1}) = 0\ ,\end{aligned} \tag{18}$$

where $\mathbf{w}^{n+1} \approx \mathbf{w}(t_{n+1})$. This problem is equipped with the boundary conditions (8)–(10) on $\partial\Omega_{t_{n+1}}$. Taking into account that $\mathcal{A}_{t_{n+1}}(\mathcal{A}_{t_i}^{-1}(x^i)) \in \Omega_{t_{n+1}}$, we can transform equations (18) completely to the domain $\Omega_{t_{n+1}}$:

$$\begin{aligned}&\frac{3\,\mathbf{u}^{n+1} - 4\,\hat{\mathbf{u}}^{n} + \hat{\mathbf{u}}^{n-1}}{2\Delta t} + \big((\mathbf{u}^{n+1} - \mathbf{w}^{n+1})\cdot\nabla\big)\,\mathbf{u}^{n+1} - \\ &\qquad - \nu\,\Delta\mathbf{u}^{n+1} + \nabla p^{n+1} = 0 \quad \text{in} \quad \Omega_{t_{n+1}}\ , \\ &\qquad \operatorname{div}\mathbf{u}^{n+1} = 0 \quad \text{in} \quad \Omega_{t_{n+1}}\ ,\end{aligned} \tag{19}$$

where $\hat{\mathbf{u}}^i = \mathbf{u}^i \circ \mathcal{A}_{t_i} \circ \mathcal{A}_{t_{n+1}}^{-1}$. This system is again equipped with the boundary conditions (8)–(10).

4.2. Space discretization

In what follows, we shall carry out the space discretization of the problem to find approximations of functions $\mathbf{u} = \mathbf{u}^{n+1}$ and $p = p^{n+1}$ defined in the domain $\Omega_{t_{n+1}}$, satisfying system (19) and boundary conditions (8)–(10). To this end, we reformulate this problem in a weak sense. Let us set $\Omega = \Omega_{t_{n+1}}$ and define the velocity spaces $W = (H^1(\Omega))^2$, $X = \{\mathbf{v} \in W; \mathbf{v}|_{\Gamma_D \cup \Gamma_{Wt}} = 0\}$ and the pressure space $M = L^2(\Omega)$. By $L^2(\Omega)$ we denote the space of square integrable functions, i.e. $L^2(\Omega) = \{v : \Omega \to R; \|v\|^2_{L^2(\Omega)} = \int_\Omega |v|^2\, dx < \infty\}$ and $H^1(\Omega)$ denotes the Sobolev space: $H^1(\Omega) = \{v \in L^2(\Omega); \frac{\partial u}{\partial x_i} \in L^2(\Omega),\ i = 1, 2\}$. In the space $H^1(\Omega)$ we define the seminorm $|\cdot|_{H^1(\Omega)}$ by $|v|^2_{H^1(\Omega)} = \int_\Omega |\nabla v|^2\, \mathrm{d}x$ Then it is possible to show that the solution $U = (\mathbf{u}, p)$ of problem (19) satisfies

$$a(U, U, V) = f(V) \quad \text{for all} \quad V = (\mathbf{v}, q) \in (X, M)\ , \tag{20}$$

where

$$\begin{aligned} a(U^*, U, V) &= \frac{3}{2\Delta t}\,(\mathbf{u}, \mathbf{v}) + \nu\,(\nabla \mathbf{u}, \nabla \mathbf{v}) + \left(\left((\mathbf{u}^* - \mathbf{w}^{n+1}) \cdot \nabla\right)\mathbf{u}, \mathbf{v}\right) - \\ &\quad - (p, \nabla \cdot \mathbf{v}) + (\nabla \cdot \mathbf{u}, q)\ , \\ f(V) &= \frac{1}{2\,\Delta t}\left(4\,\hat{\mathbf{u}}^n - \hat{\mathbf{u}}^{n-1}, \mathbf{v}\right) - \int\limits_{\Gamma_O} p_{\mathrm{ref}}\,\mathbf{v} \cdot \mathbf{n}\,\mathrm{d}S\ , \\ U &= (\mathbf{u}, p)\ , \quad V = (\mathbf{v}, q)\ , \quad U^* = (\mathbf{u}^*, p)\ . \end{aligned} \tag{21}$$

Here $(\cdot, \cdot)$ denotes the scalar product in $L^2(\Omega)$ or in $[L^2(\Omega)]^2$: $(\alpha, \beta) = \int_\Omega \alpha \cdot \beta\, \mathrm{d}x$. Moreover, we require that $\mathbf{u}$ satisfies the Dirichlet boundary conditions (8), (9). The couple $(\mathbf{u}, p)$ represents the solution on the time level t_{n+1}, i.e. $\mathbf{u}^{n+1} := \mathbf{u}$ and $p^{n+1} := p$.

In order to apply the Galerkin FEM, we shall restrict the weak formulation from the spaces W, X, M to approximate spaces W_Δ, X_Δ, M_Δ, $\Delta \in (0, \Delta_0)$, $\Delta_0 > 0$, $X_\Delta = \{\mathbf{v}_\Delta \in W_\Delta;\ \mathbf{v}_\Delta|_{\Gamma_D \cup \Gamma_{Wt}} = 0\}$. Hence, we want to find $U_\Delta = (\mathbf{u}_\Delta, p_\Delta) \in W_\Delta \times M_\Delta$ (i.e., $\mathbf{u} \in W_\Delta$, $p \in M_\Delta$) such that $\mathbf{u}_\Delta$ satisfies approximately conditions (8), (9) and

$$a(U_\Delta, U_\Delta, V_\Delta) = f(V_\Delta) \qquad \text{for all} \quad V_\Delta = (\mathbf{v}_\Delta, q_\Delta) \in X_\Delta \times M_\Delta\ . \tag{22}$$

The couple (X_Δ, M_Δ) of the finite element spaces should satisfy the *Babuška-Brezzi (BB) condition* (cf., e.g. [1], [21]), which guarantees the stability of the scheme: there exists a constant $c > 0$ such that

$$\sup_{\mathbf{w} \in X_\Delta} \frac{(p, \nabla \cdot \mathbf{w})}{|\mathbf{w}|_{H^1(\Omega)}} \geq c \|p\|_{L^2(\Omega)} \quad \text{for all} \quad p \in M_\Delta\ , \quad \Delta \in (0, \Delta_0)\ . \tag{23}$$

We proceed in the following way. We shall approximate the computational domain at time t_{n+1} by a polygonal domain. Because of simplicity we shall denote it again by Ω. By $\mathcal{T}_\Delta$ we denote a triangulation of Ω with standard properties from the FEM, formed by a finite number of closed triangles (see, e.g. [2]). The pressure space M is then approximated by the space of piecewise polynomial functions of degree $\leq k$ (= a positive integer):

$$p \approx p_\Delta \in M_\Delta = \{q \in M \cap C(\overline{\Omega}); q|_K \in P^k(K) \text{ for all } K \in \mathcal{T}_\Delta\}\ . \tag{24}$$

Here the symbol $P^k(K)$ denotes the space of all polynomials on an element K of degree $\leq k$. The velocity spaces W and X are approximated by the spaces of piecewise polynomial functions of degree $\leq k+1$:

$$\begin{aligned} \mathbf{u} \approx \mathbf{u}_\Delta \in W_\Delta = \{\mathbf{v} \in W \cap [C(\overline{\Omega})]^2; \mathbf{v}|_K \in [P^{k+1}(K)]^2 \text{ for all } K \in \mathcal{T}_\Delta\} \ , \\ X_\Delta = W_\Delta \cap X \ . \end{aligned} \tag{25}$$

The pair of the spaces defined by (24) and (25) is called the Taylor/Hood element. This couple (X_Δ, M_Δ) satisfies the BB condition (see, e.g. [1]).

In practical computations we use the Taylor/Hood P^2/P^1 elements. This means that the velocity components are piecewise quadratic functions and the pressure is a piecewise linear function.

4.3. Stabilization of the FEM

The standard Galerkin discretization (22) may produce approximate solutions suffering from spurious oscillations for high Reynolds numbers. In order to avoid this drawback, we apply the stabilization via streamline-diffusion/Petrov-Galerkin technique (see, e.g. [20], [14], [9]). We define the stabilization terms

$$\begin{aligned} \mathcal{L}_\Delta(U^*, U, V) &= \sum_{K \in \mathcal{T}_\Delta} \delta_K \left(\frac{3}{2\Delta t}\, \mathbf{u} - \nu \triangle \mathbf{u} + (\overline{\mathbf{w}} \cdot \nabla)\, \mathbf{u} + \nabla p,\, (\overline{\mathbf{w}} \cdot \nabla)\, \mathbf{v} \right)_K \ , \\ \mathcal{F}_\Delta(V) &= \sum_{K \in \mathcal{T}_\Delta} \delta_K \left(\frac{1}{2\Delta t} \left(4\, \hat{\mathbf{u}}^n - \hat{\mathbf{u}}^{n-1}\right),\, (\overline{\mathbf{w}} \cdot \nabla)\, \mathbf{v} \right)_K \ , \\ U &= (\mathbf{u}, p) \ , \quad V = (\mathbf{v}, q) \ , \quad U^* = (\mathbf{u}^*, p) \ , \end{aligned} \tag{26}$$

where the function $\overline{\mathbf{w}}$ stands for the transport velocity $\overline{\mathbf{w}} = \mathbf{u}^* - \mathbf{w}^{n+1}$, $(\cdot,\cdot)_K$ denotes the scalar product in $L^2(K)$ or $[L^2(K)]^2$ and $\delta_K \geq 0$ are suitable parameters defined later. Moreover, we introduce the pressure 'div-div' stabilization terms

$$\mathcal{P}_\Delta(U, V) = \sum_{K \in \mathcal{T}_\Delta} \tau_K (\nabla \cdot \mathbf{u}, \nabla \cdot \mathbf{v})_K \ , \qquad U = (\mathbf{u}, p) \ , \qquad V = (\mathbf{v}, q) \ , \tag{27}$$

with suitable parameters $\tau_K \geq 0$ (see relations (32)).

The *stabilized discrete problem* reads: Find $U_\Delta = (\mathbf{u}_\Delta, p_\Delta) \in W_\Delta \times M_\Delta$ such that $\mathbf{u}_\Delta$ satisfies approximately conditions (8), (9) and

$$\begin{aligned} a(U_\Delta, U_\Delta, V_\Delta) + \mathcal{L}_\Delta(U_\Delta, U_\Delta, V_\Delta) + \mathcal{P}_\Delta(U_\Delta, V_\Delta) = f(V_\Delta) + \mathcal{F}_\Delta(V_\Delta) \\ \text{for all} \quad V_\Delta \in X_\Delta \times M_\Delta \ . \end{aligned} \tag{28}$$

The parameter δ_K is defined on the basis of the transport velocity $\overline{\mathbf{w}}$ as

$$\delta_K = \delta^* \frac{\Delta_K}{2\, \max_K |\overline{\mathbf{w}}|}\, \xi(Re^{\overline{\mathbf{w}}}) \ , \tag{29}$$

where

$$Re^{\overline{\mathbf{w}}} = \frac{\Delta_K\, \max_K |\overline{\mathbf{w}}|}{2\, \nu} \tag{30}$$

is the local Reynolds number and Δ_K is the size of the element K measured in the direction of $\overline{\mathbf{w}}$. The factor $\xi(\cdot)$ is a monotonically increasing function of $Re^{\overline{\mathbf{w}}}$ such that for local advection dominance ($Re^{\overline{\mathbf{w}}} > 1$) $\xi \to 1$ and for local diffusion dominance ($Re^{\overline{\mathbf{w}}} < 1$) $\xi \to 0$. The parameter $\delta^* \in (0, 1]$ is an additional free parameter. We set, e.g.

$$\xi(Re^{\overline{\mathbf{w}}}) = \min\left(\frac{Re^{\overline{\mathbf{w}}}}{6}, 1\right) \tag{31}$$

and $\delta^* = 0.025$. The parameters τ_K are defined by

$$\tau_K = \tau^* h_K \max_K |\overline{\mathbf{w}}|\, \xi(Re^{\overline{\mathbf{w}}}) , \tag{32}$$

where $\tau^* \in (0, 1]$. In our numerical simulations we use the value $\tau^* = 1$. For theoretical analysis of such a choice we refer to [9], [14]. For other possibilities to stabilize convection-dominated problems we can refer to [12].

The nonlinear problem (28) is (on each time level) solved with the aid of the Oseen iterative process. Starting from an initial approximation $U_\Delta^{(0)}$ and assuming that already iterate $U_\Delta^{(k)}$ has been computed, we define $U_\Delta^{(k+1)} \in W_\Delta \times M_\Delta$ by

$$\begin{gathered} a(U_\Delta^{(k)}, U_\Delta^{(k+1)}, V_\Delta) + \mathcal{L}_\Delta(U_\Delta^{(k)}, U_\Delta^{(k+1)}, V_\Delta) + \mathcal{P}_\Delta(U_\Delta^{(k+1)}, V_\Delta) = f(V_\Delta) + \mathcal{F}_\Delta(V_\Delta) \\ \text{for all} \quad V_\Delta \in X_\Delta \times M_\Delta . \end{gathered} \tag{33}$$

For each time level t_{n+1} we set

$$U_\Delta^{(0)} := (2\,\hat{\mathbf{u}}^n - \hat{\mathbf{u}}^{n-1}, \hat{p}^n). \tag{34}$$

As numerical experiments show, only a few iterations (33) have to be computed on each time level.

Obviously, problem (33) is linear. It is equivalent to the linear algebraic system

$$S\,\underline{u} + 2\,\Delta t\,(B + C)\,\underline{p} = \underline{f} , \qquad B^T\,\underline{u} = 0 , \tag{35}$$

where $\underline{u} \in R^{n_\Delta}$ and $\underline{p} \in R^{m_\Delta}$ are vectors whose components represent degrees of freedom defining the velocity $\mathbf{u}_\Delta$ and the pressure p_Δ, respectively, S is a nonsingular $n_\Delta \times n_\Delta$ matrix and B and C are $n_\Delta \times m_\Delta$ matrices and $\underline{f} \in R^{n_\Delta}$. The solution of this system was realized by the direct solver UMFPACK ([5], [6], [7]), which works sufficiently fast for systems with up to 10^5 equations. For larger systems it will be necessary to apply more sophisticated techniques as, e.g. the domain decomposition approach or multilevel solvers ([22], [13]).

4.4. The solution of the structural problem

System (11) is transformed in the following way. First we rewrite this system in the form

$$\begin{aligned} m\,\ddot{h} + S_\alpha\,\ddot{\alpha} &= -\mathcal{L} - k_{hh}\,h - k_{h\alpha}\,\alpha - D_{hh}\,\dot{h} - D_{h\alpha}\,\dot{\alpha} , \\ S_\alpha\,\ddot{h} + I_\alpha\,\ddot{\alpha} &= \mathcal{M} - k_{\alpha h}\,h - k_{\alpha\alpha}\,\alpha - D_{\alpha h}\,\dot{h} - D_{\alpha\alpha}\,\dot{\alpha} . \end{aligned} \tag{36}$$

Now we express the second order derivatives $\ddot{h}$, $\ddot{\alpha}$. We get

$$\ddot{h} = \frac{1}{D}\left[-I_\alpha\,\mathcal{L} - S_\alpha\,\mathcal{M} + h\,(S_\alpha\,k_{\alpha h} - I_\alpha\,k_{hh})\,h + (S_\alpha\,k_{\alpha\alpha} - I_\alpha\,k_{h\alpha})\,\alpha + \right.$$
$$\left. + (S_\alpha\,D_{\alpha h} - I_\alpha\,D_{hh})\,\dot{h} + (S_\alpha D_{\alpha\alpha} - I_\alpha D_{h\alpha})\,\dot{\alpha}\right]\,,$$
$$\ddot{\alpha} = \frac{1}{D}\left[S_\alpha\,\mathcal{L} + m\,\mathcal{M} + (S_\alpha\,k_{hh} - m\,k_{\alpha h})\,h + (S_\alpha\,k_{h\alpha} - m\,k_{\alpha\alpha})\,\alpha + \right.$$
$$\left. + (S_\alpha\,D_{hh} - m\,D_{\alpha h})\,\dot{h} + (S_\alpha\,D_{h\alpha} - m\,D_{\alpha\alpha})\,\dot{\alpha}\right]\,,$$

where

$$D = m\,I_\alpha - S_\alpha^2\,.$$

It is necessary to assume that $D \neq 0$. The transformation $y_1 = h$, $y_2 = \dot{h}$, $y_3 = \alpha$, $y_4 = \dot{\alpha}$ leads to the first order system

$$\dot{\mathbf{Y}} = \begin{pmatrix} \dot{y}_1 \\ \dot{y}_2 \\ \dot{y}_3 \\ \dot{y}_4 \end{pmatrix} = \mathbf{f}(t, \mathbf{Y}(t)) =$$
$$= \begin{pmatrix} y_2 \\ \frac{1}{D}\left[-I_\alpha\,\mathcal{L} - S_\alpha\,\mathcal{M} + (S_\alpha\,k_{\alpha h} - I_\alpha\,k_{hh})\,y_1 + (S_\alpha\,k_{\alpha\alpha} - I_\alpha\,k_{h\alpha})\,y_3 + \right. \\ \left. + (S_\alpha\,D_{\alpha h} - I_\alpha\,D_{hh})\,y_2 + (S_\alpha\,D_{\alpha\alpha} - I_\alpha\,D_{h\alpha})\,y_4\right] \\ y_4 \\ \frac{1}{D}\left[S_\alpha\,\mathcal{L} + m\,\mathcal{M} + (S_\alpha\,k_{hh} - m\,k_{\alpha h})\,y_1 + (S_\alpha\,k_{h\alpha} - m\,k_{\alpha\alpha})\,y_3 + \right. \\ \left. + (S_\alpha\,D_{hh} - m\,D_{\alpha h})\,y_2 + (S_\alpha\,D_{h\alpha} - m\,D_{\alpha\alpha})\,y_4\right] \end{pmatrix} = \tag{37}$$
$$= \widehat{\mathbf{Q}}\,\mathbf{Y} + \mathbf{R}\,,$$

with the matrix $\widehat{\mathbf{Q}}$ and vector $\mathbf{R}$ defined by

$$\widehat{\mathbf{Q}} = \begin{pmatrix} 0 & 1 & 0 & 0 \\ \frac{S_\alpha\,k_{\alpha h} - I_\alpha\,k_{hh}}{D} & \frac{S_\alpha\,D_{\alpha h} - I_\alpha\,D_{hh}}{D} & \frac{S_\alpha\,k_{\alpha\alpha} - I_\alpha\,k_{h\alpha}}{D} & \frac{S_\alpha\,D_{\alpha\alpha} - I_\alpha\,D_{h\alpha}}{D} \\ 0 & 0 & 0 & 1 \\ \frac{S_\alpha\,k_{hh} - m\,k_{\alpha h}}{D} & \frac{S_\alpha\,D_{hh} - m\,D_{\alpha h}}{D} & \frac{S_\alpha\,k_{h\alpha} - m\,k_{\alpha\alpha}}{D} & \frac{S_\alpha\,D_{h\alpha} - m\,D_{\alpha\alpha}}{D} \end{pmatrix}\,, \tag{38}$$
$$\mathbf{R} = \frac{1}{D}\begin{pmatrix} 0 \\ -I_\alpha\,\mathcal{L} - S_\alpha\,\mathcal{M} \\ 0 \\ S_\alpha\,\mathcal{L} + m\,\mathcal{M} \end{pmatrix}\,.$$

System (37) is solved by the second order Runge-Kutta method. The approximate solution $\mathbf{Y}_{n+1}$ at time instant t_{n+1} is computed with the aid of the formula

$$\mathbf{Y}_{n+1} = \mathbf{Y}_n + \Delta t\,\mathbf{f}\left(t_{n+\frac{1}{2}}, \mathbf{Y}_n + \frac{1}{2}\,\Delta t\,\mathbf{f}(t_n, \mathbf{Y}_n)\right)\,. \tag{39}$$

The function $\mathbf{f}$ is evaluated at the time instant $t_{n+1/2}$ in the following way. From the solution $\mathbf{u}_\Delta$ computed already on time levels t_n a t_{n-1} the values $\mathcal{L}_{n-1}$, $\mathcal{L}_n$ of the vertical force $\mathcal{L}$ and $\mathcal{M}_{n-1}$, $\mathcal{M}_n$ of the moment $\mathcal{M}$ are computed. Then, by extrapolation, $\mathcal{L}$ and $\mathcal{M}$ are evaluated at time $t_{n+1/2} = t_n + \Delta t/2$:

$$\mathcal{L}_{n+\frac{1}{2}} = \mathcal{L}_n + \frac{1}{2}\left(\mathcal{L}_n - \mathcal{L}_{n-1}\right) \ ,$$
$$\mathcal{M}_{n+\frac{1}{2}} = \mathcal{M}_n + \frac{1}{2}\left(\mathcal{M}_n - \mathcal{M}_{n-1}\right) \ ,$$

which are used for the computation of the function $\mathbf{f}(t_{n+1/2}, \cdot)$.

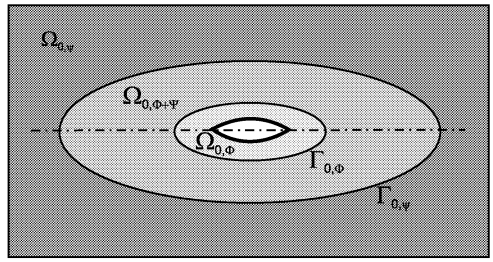

Fig.3: Partition of the domain Ω_0

5. Realization of the ALE mapping

There exist several possibilities of the construction of the ALE mapping for the flow around an oscillating airfoil. For example, in [19] we describe the ALE mapping in the case of an isolated airfoil. The situation is more complex, if the airfoil is inserted into a channel. Here we describe a simple and efficient construction of the ALE mapping, which was used in our computations.

We start from the reference domain Ω_0 (initial configuration). Provided we know the functions $h(t)$ and $\alpha(t)$, $t \in [0, T]$, we want to construct the one-to-one ALE mapping $\mathcal{A}_t$ of $\bar{\Omega}_0$ onto $\bar{\Omega}_t$. We proceed in the following way. The reference domain Ω_0 is divided in three subdomains by two ellipses with center at the elastic axis of the airfoil. We denote them $\Omega_{0,\Phi}$ (interior subdomain containig the airfoil), $\Omega_{0,\Psi}$ (the exterior subdomain adjacent to fixed impermeable walls of the channel, inlet and outlet) and $\Omega_{0,\Phi+\Psi}$ (the subdomain between $\Omega_{0,\Phi}$ and $\Omega_{0,\Psi}$). See Figure 3.

The ALE mapping consists of suitable mappings representing the deformation of the domains $\Omega_{0,\Phi+\Psi}$, $\Omega_{0,\Phi}$ and $\Omega_{0,\Psi}$. We assume that the domain $\Omega_{0,\Phi}$ moves as a solid body together with the airfoil $\Gamma_{\mathrm{W}t}$, whose position is determined by the displacement h and the rotation angle α:

$$\begin{aligned} x_1 &= (X_1 - X_1^{\mathrm{EO}})\cos\alpha + (X_2 - X_2^{\mathrm{EO}})\sin\alpha + X_1^{\mathrm{EO}} \ , \\ x_2 &= -(X_1 - X_1^{\mathrm{EO}})\sin\alpha + (X_2 - X_2^{\mathrm{EO}})\cos\alpha + h + X_2^{\mathrm{EO}} \ , \end{aligned} \tag{40}$$

where X_1^{EO}, X_2^{EO} are the reference coordinates of the elastic axis (at time $t = 0$). We denote this mapping by Φ. Therefore, we set

$$x = \mathcal{A}_t(X) = \Phi(X) \quad \text{for} \quad X \in \Omega_{0,\Phi} \ . \tag{41}$$

Further, we assume that the domain $\Omega_{0,\Psi}$ does not depend on time. This means that we set

$$x = \mathcal{A}_t(X) = \Psi(X) = X \quad \text{for} \quad X \in \Omega_{0,\Psi} \ . \tag{42}$$

The domain $\Omega_{0,\Phi+\Psi}$ is transformed by the formula

$$\mathcal{A}_t = (1-\theta)\,\Phi + \theta\,\Psi \quad \text{in} \quad \Omega_{0,\Phi+\Psi} \ , \tag{43}$$

where $\theta \in [0,1]$ depends on X.

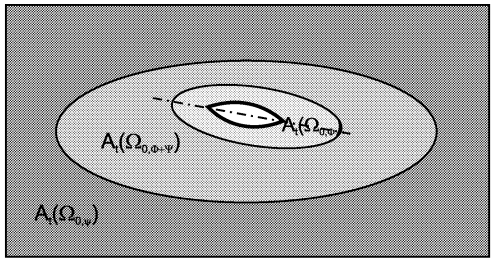

Fig.4: Partition of the domain $\mathcal{A}_t(\Omega_0)$ at time t

By $\Gamma_{0,\Phi}$ we denote the ellipse, which forms the interface between the domains $\Omega_{0,\Phi}$ and $\Omega_{0,\Phi+\Psi}$. Further, the ellipse between the domains $\Omega_{0,\Phi+\Psi}$ and $\Omega_{0,\Psi}$ will be denoted by $\Gamma_{0,\Psi}$. These ellipses are chosen so that

$$\frac{a_\Psi}{b_\Psi} = \frac{a_\Phi}{b_\Phi} \ , \tag{44}$$

where a_Ψ and a_Φ are the lengths of the semimajor axis of the ellipses $\Gamma_{0,\Psi}$ and $\Gamma_{0,\Phi}$, respectively. By b_Ψ and b_Φ we denote the length of the semiminor axis of $\Gamma_{0,\Psi}$ and $\Gamma_{0,\Phi}$, respectively. In the domain Ω_0 we define the function

$$C(X) = \sqrt{\frac{1}{a_\Phi^2}\,(X_1 - X_1^{\mathrm{EO}})^2 + \frac{1}{b_\Phi^2}\,(X_2 - X_2^{\mathrm{EO}})^2} \ , \qquad X \in \Omega_0 \ . \tag{45}$$

Under the above notation, we have

$$C(X) < 1 \qquad \text{for} \quad X \in \Omega_{0,\Phi} \ , \tag{46}$$

$$C(X) > 1 \quad \text{and} \quad C(X) < \frac{a_\Psi}{a_\Phi} \qquad \text{for} \quad X \in \Omega_{0,\Phi+\Psi} \ , \tag{47}$$

$$C(X) > \frac{a_\Psi}{a_\Phi} \qquad \text{for} \quad X \in \Omega_{0,\Psi} \tag{48}$$

and

$$C(X) = 1 \qquad \text{for} \quad X \in \Gamma_{0,\Phi} \ , \tag{49}$$

$$C(X) = \frac{a_\Psi}{a_\Phi} \qquad \text{for} \quad X \in \Gamma_{0,\Psi} \ . \tag{50}$$

Now, the function θ appearing in (43) is defined by

$$\theta(X) = \frac{1}{\dfrac{a_\Psi}{a_\Phi} - 1}\ \min\left(\max(C(X) - 1,\, 0),\, \frac{a_\Psi}{a_\Phi} - 1\right) \ . \tag{51}$$

It is obvious, that the above definition of the ALE mapping can be applied provided the deformation defined by the functions h and α is not too large.

The ALE velocity $\mathbf{w}$ is approximated at time t_{n+1} by the function defined as

$$\mathbf{w}^{n+1}(x) = \frac{3\,x - 4\,\mathcal{A}_n(\mathcal{A}_{n+1}^{-1}(x)) + \mathcal{A}_{n-1}(\mathcal{A}_{n+1}^{-1}(x))}{2\,\Delta t}\,, \qquad x \in \Omega_{n+1}\,. \tag{52}$$

6. Numerical results

The method described above was applied to the numerical solution of the problem, which was analyzed experimentally in the wind tunnel of the Institute of Thermomechanics of the Academy of Sciences of the Czech Republic in Prague (see [10]).

The airfoil is symmetric and its boundary is formed by two circular arcs with parameters given (in milimeters) in Figure 5. The position of the elastic axis EO is at one third of the chord of the airfoil, measured from the leading edge. The maximum height of the wind tunnel measurement section is 210 mm. The results of the test problem were obtained for the height equal to 180 mm. The following parameters from [10] were used:

$$\begin{gathered}
k_{hh} = 1711.6\,\mathrm{N/m}\,, \qquad k_{\alpha\alpha} = 4.5\,\mathrm{Nm/rad}\,,\\
k_{h\alpha} = 0.0\,\mathrm{N/rad}\,, \qquad k_{\alpha h} = 0.0\,\mathrm{N}\\
m = 0.0821\,\mathrm{kg}\,,\\
S_\alpha = -0.00013\,\mathrm{kgm}\,, \qquad I_\alpha = 0.000095\,\mathrm{kgm}^2\,,\\
D_{hh} = 5.0\,\mathrm{Ns/m}\,, \qquad D_{\alpha\alpha} = 0.003\,\mathrm{Nms/rad}\,,\\
D_{h\alpha} = 0.0\,\mathrm{Ns/rad}\,, \qquad D_{\alpha h} = 0.0\,\mathrm{Ns/m}\,,\\
\ell = \text{depth of the airfoil} = 0.08\,\mathrm{m}\,.
\end{gathered} \tag{53}$$

The parameter S_α is negative, which means that the center of gravity of the airfoil is closer to the leading edge than the elastic axis.

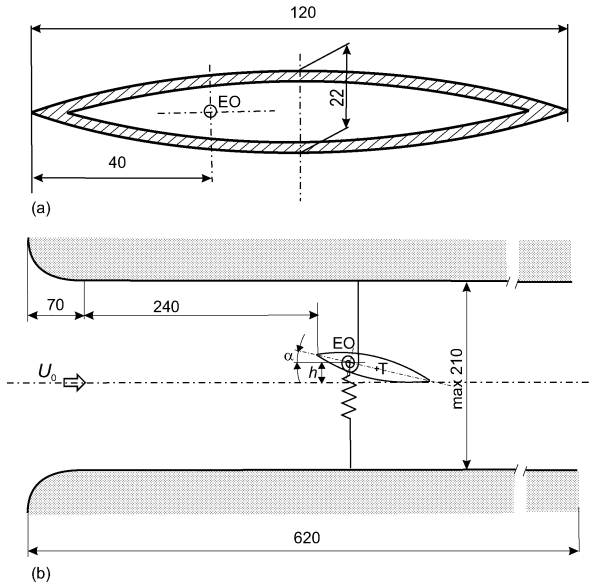

Fig.5: Geometry of the airfoil and wind tunnel

By the solution of the coupled system (19) and (37), we obtain among other the dependence of the displacement h and the torsion angle α on time. Then the frequency analysis is carried out with the aid of the Fourier transform

$$G(f_n) = \int_0^T g(t)\, \mathrm{e}^{-2\pi\, \mathrm{i}\, f_n\, t}\, \mathrm{d}t$$

with $g = h$ or $g = \alpha$ and $f_n = n\,\Delta f \in [0, 50]$, $\Delta f = 0.1\,\mathrm{Hz}$, approximated by the rectangle formula

$$G(f_n) = \sum_{k=0}^{N-1} g(t_k)\, \mathrm{e}^{-2\pi\, \mathrm{i}\, f_n\, t_k}\, \Delta t\ .$$

Here i is the imaginary unit, $\Delta t = T/N$ and N is the number of time steps in the interval $[0, T)$. The results of the frequency analysis are shown in graphs of the quantity

$$|G(f_n)| = \sqrt{\mathrm{Re}^2\,(G(f_n)) + \mathrm{Im}^2(G(f_n))}\ .$$

The resonance frequences $f1$ and $f2$ are defined in our computations as maximum points of the function $|G|$ corresponding to $g = \alpha$ and $g = h$, respectively. The frequences $f1$ and $f2$ obtained in the experiment described in [11] for the functions α and h are shown in Figure 6 in dependence on the inlet flow velocity.

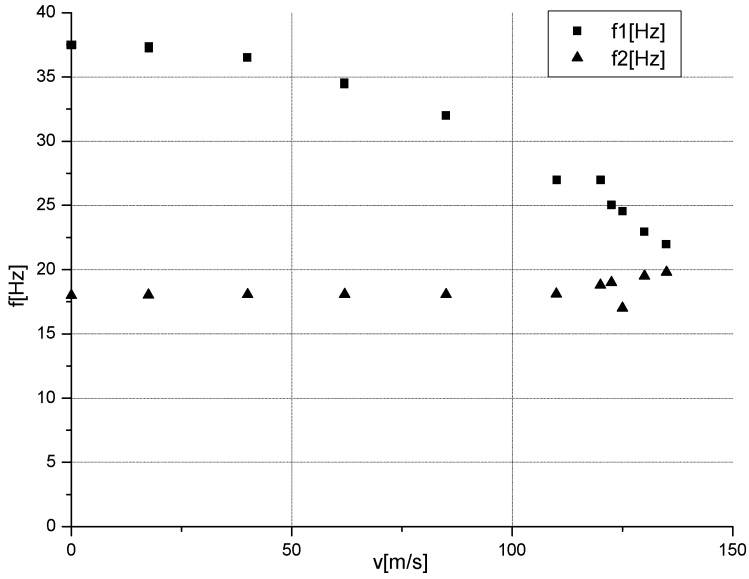

Fig.6: Resonance frequencies obtained by experiment

6.1. Solution without the influence of the fluid

First, we do not consider the influence of the fluid on airfoil vibrations. This means that we solve system (11) with zero right-hand side (which corresponds to $\mathcal{L} = 0$ and $\mathcal{M} = 0$).

The initial conditions are chosen as $\alpha(0) = 2.86°$, $h(0) = 6\,\text{mm}$ and zero initial derivatives. The solution of this sytem is given by the eigenvalues

$$s_{1,3} = -22.397 \pm 142.638\,\text{i}\,, \qquad s_{2,4} = -12.846 \pm 217.637\,\text{i}\,,$$

of the matrix $\widehat{\mathbf{Q}}$ from (38), obtained for the parameters (53). The corresponding frequences $f2 = 22.7\,\text{Hz}$ and $f1 = 34.64\,\text{Hz}$, are given by the formulae $f2 = \text{Im}(s_1)/(2\pi)$, $f1 = \text{Im}(s_2)/(2\pi)$. The functions $h(t)$ and $\alpha(t)$ computed numerically by the Runge-Kutta method are shown in Figure 7. The frequency analysis shown in Figure 8 yields the resonance frequencies 22.95 Hz a 34.8 Hz. We see that the maximum relative computational error is 1 %.

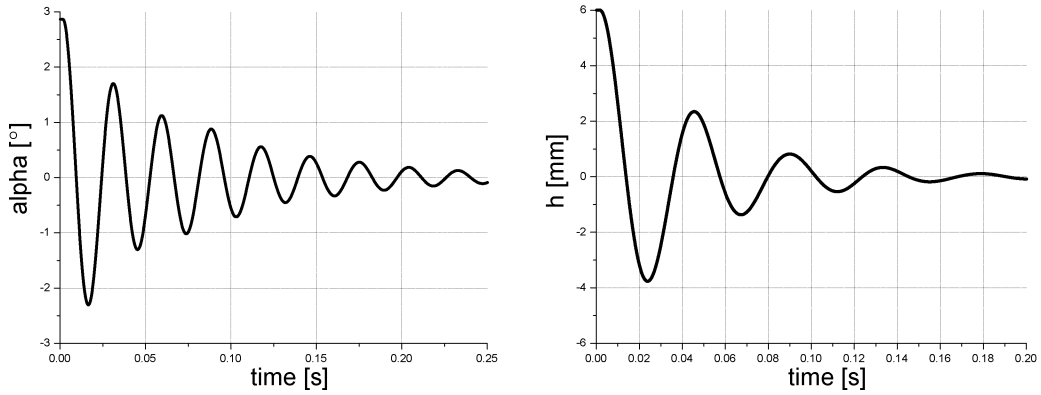

Fig.7: $\alpha(t)$ (left) and $h(t)$ (right) for the computation without the influence of the fluid

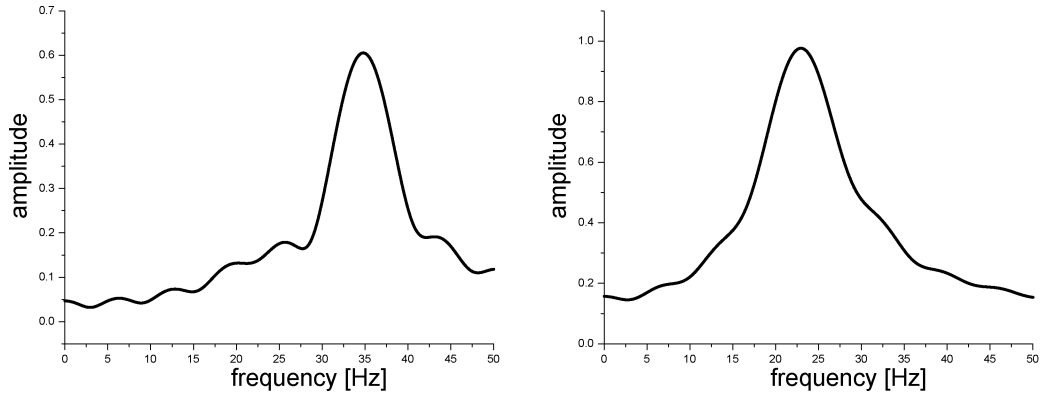

Fig.8: Frequency spectra for $\alpha(t)$ (left) and $h(t)$ (right) without the influence of the fluid

6.2. Flow induced airfoil vibrations

Now we shall be concerned with the complete coupled flow induced airfoil vibrations. The triangulation of the domain Ω_0 was obtained by the program ANGENER (see [3]), which allows the construction of a mesh anisotropically refined in the boundary layer and wake. The computation started from the isotropic mesh shown in Figure 9. During the

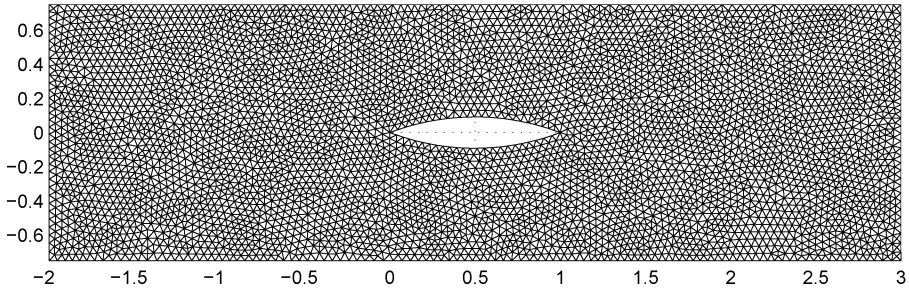

Fig.9: Isotropic initial triangulation

computational process this triangulation was refined by the program ANGENER separately for each Reynolds number.

The solution of the flow problem was carried out with the use of the dimensionless formulation by the stabilized P_2/P_1 finite element method described in Section 4 with the stabilization parameters

$$\delta^* = 0.025\ , \qquad \tau^* = 1$$

and the dimensionless time step

$$\Delta t_{\mathrm{dimless}} = 0.025\ .$$

In what follows, we present the obtained results for several inlet flow velocities.

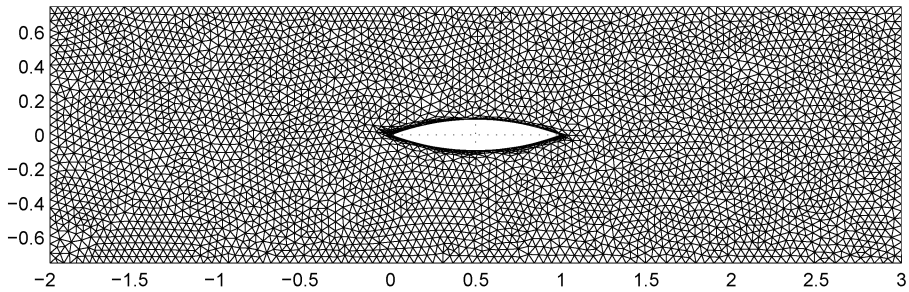

Fig.10: Anisotropic mesh for the inlet flow velocity 0 ms^{-1}

6.2.1. Inlet flow velocity 0 ms^{-1}

For the inlet velocity 0 ms^{-1} the mesh was refined in the vicinity of the airfoil only as shown in Figure 10. The initial position of the airfoil is given by coordinates $\alpha = 2.86°$ and $h = 6$ mm.

The results are shown in Figures 11 and 12. The resonance frequences for h and α are 22.8 Hz and 34.75 Hz, respectively. The first resonance belongs to a predominantly vertical motion of the airfoil, while in the second resonance the rotation of the airfoil prevails.

6.2.2. Inlet flow velocity 17.5 ms^{-1} – Re = 140000

In the numerical analysis we started from the isotropic triangulation from Figure 9, which was successively adapted by the program ANGENER. The resulting mesh is shown

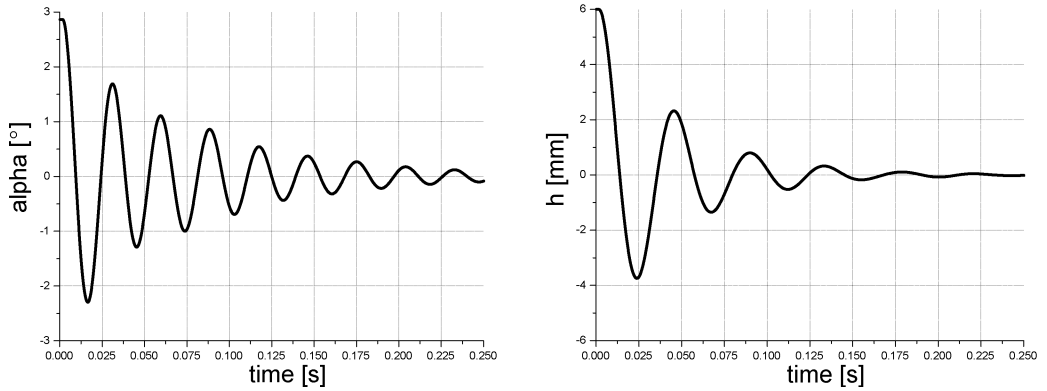

Fig.11: $\alpha(t)$ (left) and $h(t)$ (right) for the inlet flow velocity 0 ms^{-1}

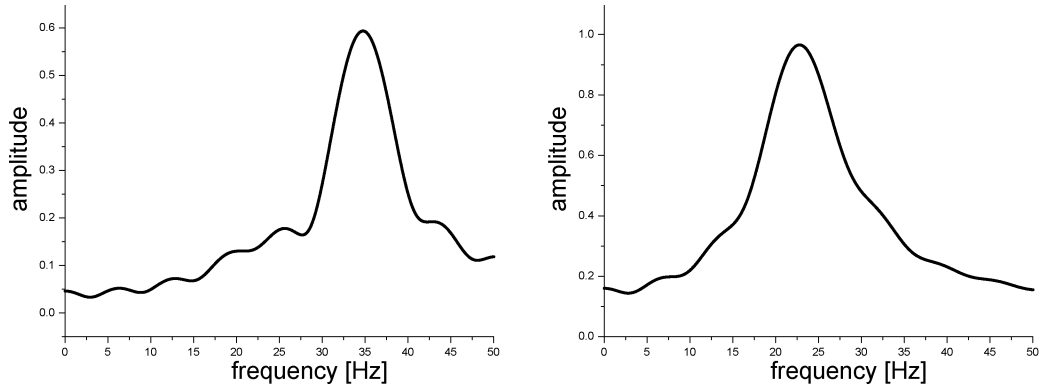

Fig.12: Frequency spectra for $\alpha(t)$ (left) and $h(t)$ (right) for zero inlet flow velocity

in Figure 13. The computed signals for α and h are plotted in Figure 14, the results of the frequency analysis are seen in Figure 15. The resonance frequences are 36.0 Hz and 24.25 Hz.

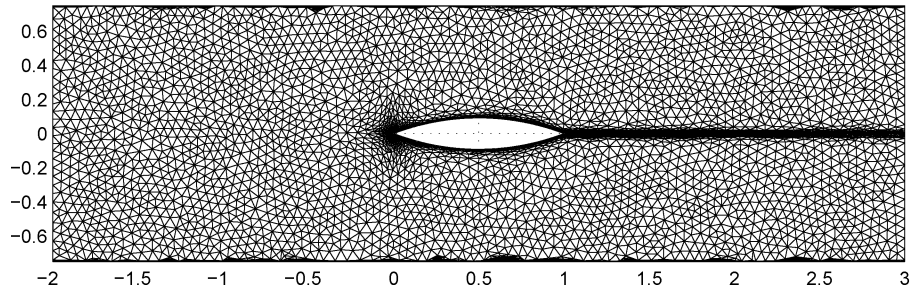

Fig.13: Anisotropic mesh for the case with the inlet flow velocity 17.5 ms^{-1}, 10151 vertices and 18647 elements

6.2.3. Inlet flow velocity 40 ms^{-1} – Re = 320000

The anisotropic adapted mesh is shown in Figure 16 The initial position of the airfoil is given by the values $\alpha = 3.43775°$ and $h = -3.6$ mm. The results are shown in Figures 17 and 18. The resonance frequencies are 37.4 Hz and 22.0 Hz.

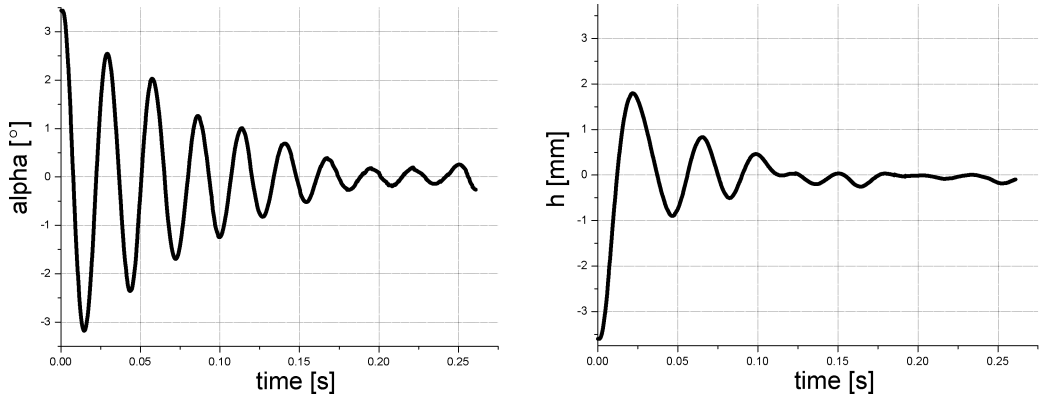

Fig.14: $\alpha(t)$ (left) and $h(t)$ (right) for the inlet flow velocity 17.5 ms^{-1}

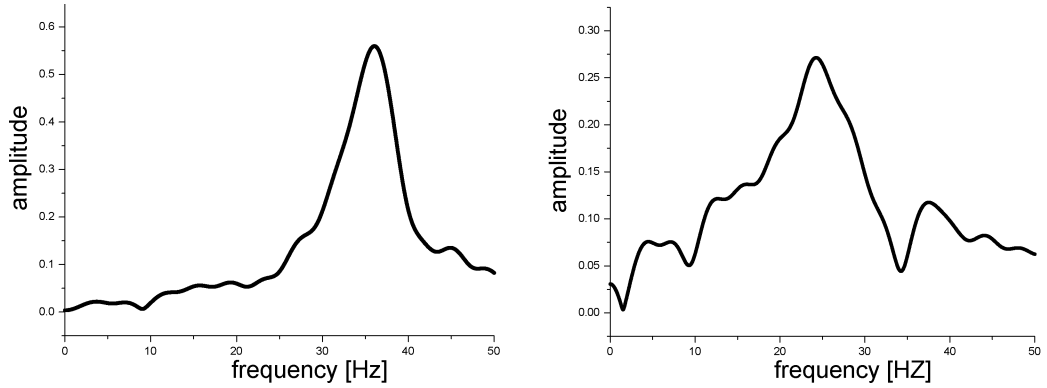

Fig.15: Frequency spectra for $\alpha(t)$ (left) and $h(t)$ (right) for the inlet flow velocity 17.5 ms^{-1}

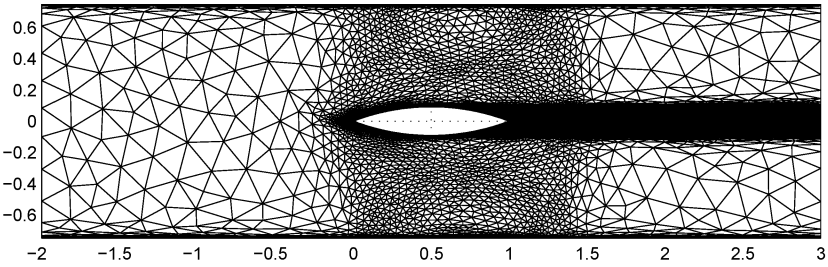

Fig.16: Anisotropic adapted mesh for the inlet flow velocity 40 ms^{-1}

6.2.4. Inlet flow velocity 60 ms^{-1} – Re = 480000

Figure 19 shows the graphs of the functions $\alpha(t)$ and $h(t)$ for the inlet flow velocity 60 ms^{-1}. In Figure 20 we see the frequency spectra for $\alpha(t)$ and $h(t)$.

6.2.5. Inlet flow velocity 80 ms^{-1} – Re = 640000

Figure 21 shows the graphs of the functions $\alpha(t)$ and $h(t)$ for the inlet flow velocity 80 ms^{-1}. In Figure 22 we see the frequency spectra for $\alpha(t)$ and $h(t)$.

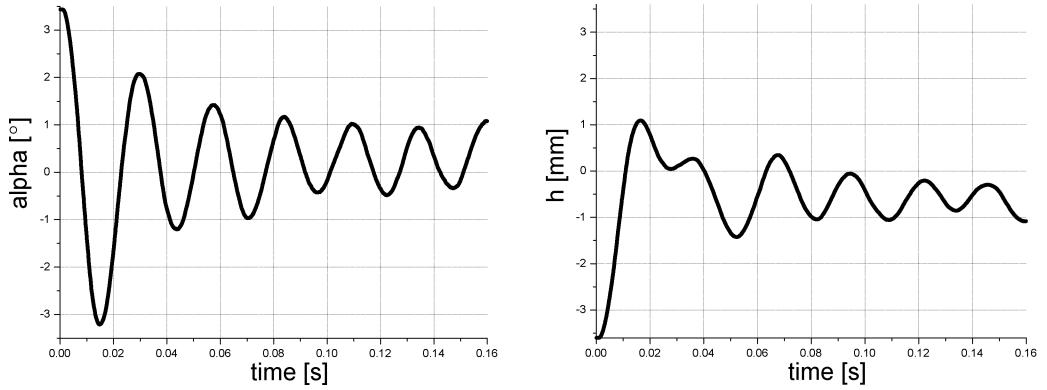

Fig.17: $\alpha(t)$ (left) and $h(t)$ (right) for the inlet flow velocity 40 ms^{-1}

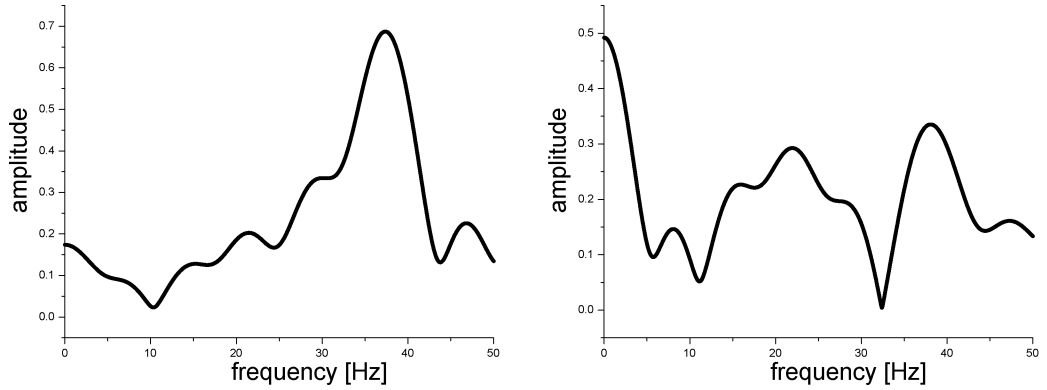

Fig.18: Frequency spectrum for $\alpha(t)$ (left) and $h(t)$ (right) for the inlet flow velocity 40 ms^{-1}

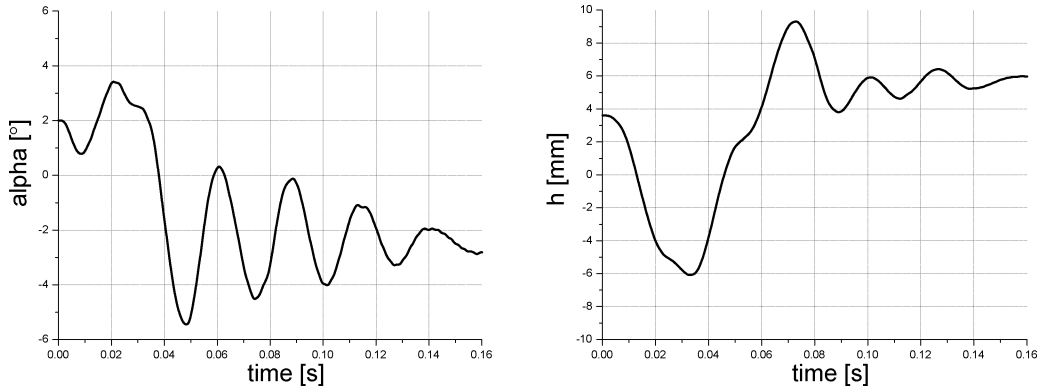

Fig.19: $\alpha(t)$ (left) and $h(t)$ (right) for the inlet flow velocity 60 ms^{-1}

6.2.6. Comparison of results with experiment

Figure 23 shows the comparison of resonance frequencies obtained by experiment and evaluated from the numerical simulation of the airfoil vibration in time domain. We see that

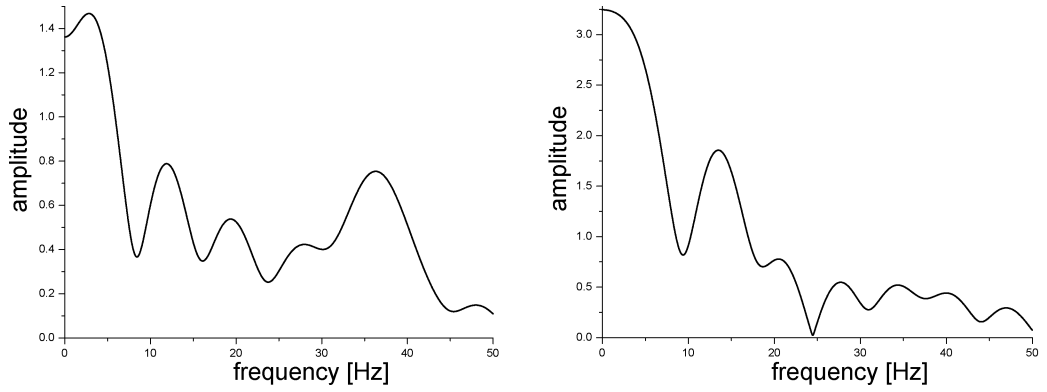

Fig.20: Frequency spectra for $\alpha(t)$ (left) and $h(t)$ (right) for the inlet flow velocity 60 ms^{-1}

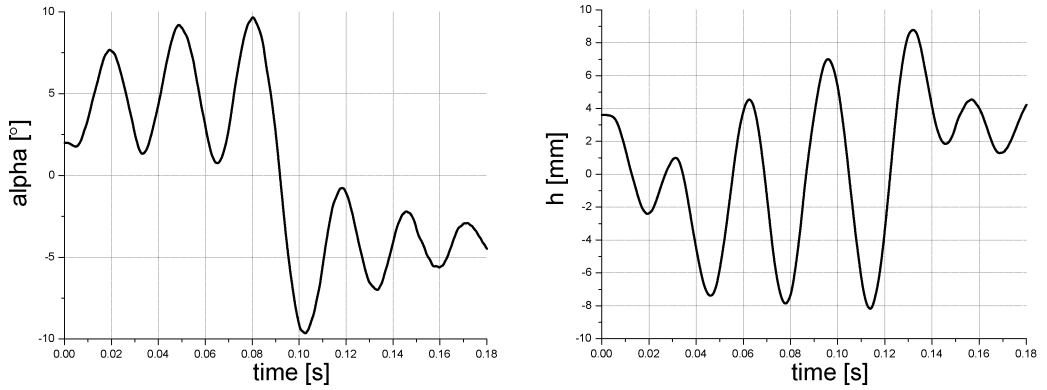

Fig.21: $\alpha(t)$ (left) and $h(t)$ (right) for the inlet flow velocity 80 ms^{-1}

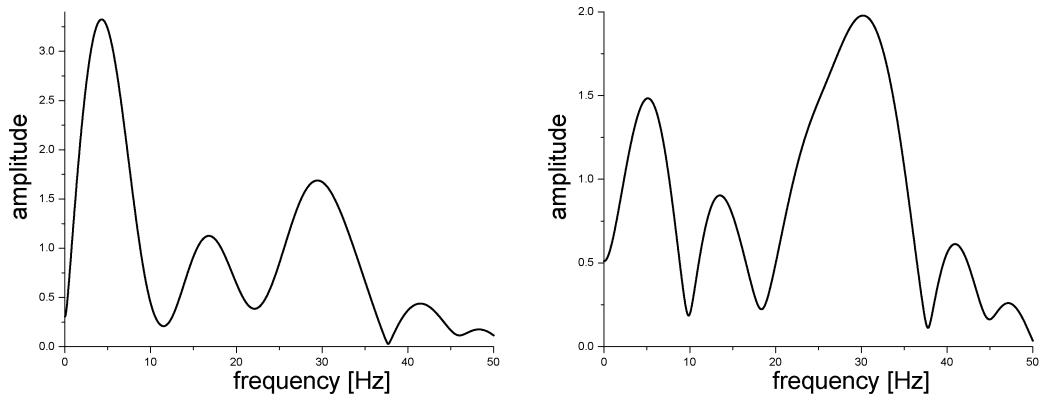

Fig.22: Frequency spectra for $\alpha(t)$ (left) and $h(t)$ (right) for the inlet flow velocity 80 ms^{-1}

the agreement is very good. By increasing the inlet flow velocity the resonance frequences are getting close together, which is a typical behaviour for pre-flutter regimes of airfoil vibration, when the coupling between the rotation and translation of the airfoil becomes stronger ([4]).

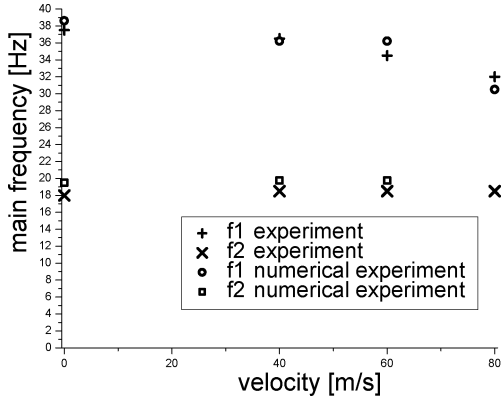

Fig.23: Comparison of resonance frequencies obtained by experiment and numerical simulation

7. Conclusion

In this paper the numerical method for the simulation of the interaction of viscous incompressible channel flow and a vibrating airfoil is developed. The method contains several important ingredients:

- ALE method for the treatment of the time dependent computational domain,
- time discretization using the second-order backward difference formula,
- space discretization by the stabilized finite elements, satisfying the Babuška–Brezzi condition,
- suitable construction of the ALE mapping.

The method was applied to the numerical simulation of flow induced vibrations of a double circle airfoil inserted in a wind tunnel. The computational results were compared with wind tunnel experiments. The agreement of the computational and experimental results is very satisfactory.

The next step in the research will be the investigation of turbulence models included in the described technique. We have in mind standard one equation or two equation models popular in technical practice (e.g., the Spalart-Allmaras model [18] or the widely used $k-\varepsilon$ model treated, e.g. in [17], Section 10). From the point of view of practical applications it will be suitable to increase the speed of the computational process by the use of the domain decomposition method and a parallelization of the algorithm.

Acknowledgements

This research was supported under the grant No. IAA200760613 of the Grant Agency of the Academy of Sciences of the Czech Republic. It was also partly supported under the Research Plans MSM 0021620839 (M. Feistauer) and 6840770003 (P. Sváček) of the Ministry of Education of the Czech Republic and the project No. 48607 of the Grant Agency of the Charles University in Prague (M. Růžička).

References

[1] Brezzi F., Falk R.S.: Stability of higher-order Hood-Taylor methods, SIAM J. Numer. Anal. 28 (1991), 581–590

[2] Ciarlet P.G.: The Finite Element Method for Elliptic Problems, North-Holland, Amsterdam, 1979

[3] Dolejší V.: ANGENER V3.0, http://adela.karlin.mff.cunicz/˜dolejsi/angen/angen.htm, Charles University Prague, Faculty of Mathematics and Physics.

[4] Dowell E.H.: A Modern Course in Aeroelasticity, Kluwer Academic Publishers, Dodrecht (1995)

[5] Davis T.A.: UMFPACK V4.0, http://www.cise.ufl.edu/research/sparse/unfpack, University of Florida

[6] Davis T.A.: A column pre-ordering strategy for the unsymmetric-pattern multifrontal method, ACM Trans. Math. Software 30 (2004), 165–195

[7] Davis T.A., Duff I.S.: A combined unifrontal/multifrontal method for unsymmetric sparse matrices, ACM Trans. Math. Software 25 (1999), 1–19

[8] Feistauer M.: Mathematical Methods in Fluid Dynamics, Logman Scientific & Technical, Harlow, (1993)

[9] Gelhard T., Lube G., Olshanskii M.A., Starcke J.-H.: Stabilized finite element schemes with LBB-stable elements for incompressible flows, J. Comput. Appl. Math. 177 (2005), 243–267

[10] Horáček J., Kozánek J., Veselý J.: Dynamic and stability properties of an aeroelastic model, In: Engineering Mechanics 2005, Svratka 9–12 May 2005, Institute of Thermomechanics of the Academy of Sciences, Prague 2005, 121–122 (CD-ROM, 12 pages) [ISBN 80-85918-93-5]

[11] Horáček J., Luxa M., Vaněk F., Veselý J., Vlček V.: Design of an experimental set-up for the study of unsteady 2D aeroelastic phenomena by optical methods, Research Report of the Institute of Thermomechanics of AS CR Prague, No. Z 1347/04, November 2004 (in Czech)

[12] John V., Knobloch P.: On spurious oscillations at layers diminishing (SOLD) methods for convection-diffusion equations: Part I – A review, Comput. Methods Appl. Mech. Engrg. 196 (2007), 2197–2215

[13] John V., Knobloch P., Matthies G., Tobiska L.: Non-nested multi-level solvers for finite element discretizations of mixed problems, Computing 68 (2002), 313–341

[14] Lube G.: Stabilized Galerkin finite element methods for convection dominated and incompressible flow problems, Num. Anal. and Math. Model., Banach Center publications 29 (1994), 85–104

[15] Naudasher E., Rockwell D.: Flow-Induced Vibrations, A.A. Balkema, Rotterdam (1994)

[16] Nomura T., Hughes T.J.R.: An arbitrary Lagrangian-Eulerian finite element method for interaction of fluid and a rigid body, Comput. Methods Appl. Mech. Engrg. 95 (1992), 115–138

[17] Pope S.B.: Turbulent Flows, Cambridge University Press, Cambridge (2005)

[18] Spalart P.R., Allmaras S.R.: A one equation turbulence model for aerodynamic flows, Recherche Aérospatiale 1 (1994), 5–21

[19] Sváček P., Feistauer M., Horáček J.: Numerical simulation of flow induced airfoil vibrations with large amplitudes, Journal of Fluids and Structures 23 (2007), 391–411

[20] Turek S.: Efficient Solvers for Incompressible Flow Problems, Springer, Berlin (1998)

[21] Verfürth R.: Error estimates for mixed finite element approximation of the Stokes equations, R.A.I.R.O. Analyse numérique/Numerical analysis 18(2) (1984), 175–182

[22] Quarteroni A., Valli A.: Domain Decomposition Methods for Partial Differential Equations, Oxford Science Publications, Oxford (1999)

Received in editor's office: November 10, 2007
Approved for publishing: February 13, 2008